EFFECT OF IMAGE MATCHING WINDOW SIZE ON SATELLITE JITTER FREQUENCY DETECTION

Han Zhang[1], Shijie Liu [1*] , Zhen Ye [1], Xiaohua Tong[1] , Huan Xie[1] , Shouzhu Zheng[1], Qian Du [1]

[1] College of Surveying and Geo-Informatics, Tongji University, Shanghai 200092, China
(1811489, liusjtj, 89_yezhen, xhtong, huanxie, shouzhuzheng, du) @tongji.edu.cn

Commission I, WG I/4

KEY WORDS: High resolution satellite, Satellite jitter, Dynamic imaging model, Multi-temporal image, Matching window size, Jitter detection

ABSTRACT:

Satellite attitude jitter is a common and complex phenomenon for high-resolution satellites and it is detectable by multi-temporal image matching. This paper analyses the effect of image matching window size on jitter frequency detection. First, two simulation images with a given short time lag and line scanning frequency affected by a modelled jitter are generated based on the principle of dynamic imaging model. Then, the relative image distortions are obtained by dense image matching with different matching window size and the frequency is estimated through spectrum analysis of the obtained image distortions. The experimental results demonstrated the feasibility and reliability of high frequency jitter detection based on dense image matching, and the results indicated that the maximum detectable frequency is almost not affected by the change of image matching window size, which provided useful demonstration of image-based satellite jitter detection capacity.

1. INTRODUCTION

With the development of earth observation technology, High-resolution satellite images (HRSIs) has been widely used in the fields of land resources exploration, city planning, the establishment and renewal of national basic geographic information database etc(Yang et al., 2017). However, attitude jitter, which refers to the periodic instability of attitude caused by the micro-vibration of satellite platform, affects geometric quality and imaging performance of high-resolution satellites. And it is an inevitable issue as the jitter can be induced by both the external space environment and internal mechanical operation, and the frequencies and amplitudes of jitters for different satellites are diverse (Wang et al., 2016). Many domestic and foreign satellites, such as IKONOS, High Resolution Imaging Science Experiment (HiRISE), ZiYuan-3, YaoGan-26 and GaoFen-9, have been affected by the attitude jitter (Grodecki, Dial, 2003; Mattson et al., 2009; Tong et al., 2014; Liu et al., 2016; Wang et al., 2016a, 2016b; Pan et al.,2016; (Wang et al., 2017; Zhang, Guan, 2018).

Nowadays, the published methods of jitter detection can be categorized into two categories. One is dependent on a high-performance attitude-measuring sensor since the attitude oscillation is the direct manifestation of jitter(Takaku, Tadono, 2009). The data of high-frequency angular displacement sensor were fused with satellite sensor attitude data for the jitter detection of YaoGan-26 satellite (Wang et al., 2017). After obtaining the high frequency angular displacement information through processing the measurements of the micro-vibration accelerometer installed on the GF-9 satellite, they corrected the attitude by taking the high-frequency attitude correction into account in the geometric model. And after the jitter correction, the jitter amplitude decreased from 0.9 pixels to 0.4 pixels (Zhang, Guan, 2018).

The other is based on imagery to obtain the distortion caused by satellite jitter, such as multispectral imagery, staggered CCD (Charge Coupled Device) images, and stereo image pairs, ortho-images, or linear objects in images. The attitude jitter detection method based on the parallax observation configuration were proposed, which estimated attitude jitter from the relative registration errors of adjacent bands of ASTER short-wave infrared sensor (Teshima, Iwasaki, 2008). Similar methods were used for detecting jitter of many satellites, such as HiRISE, Mapping Satellite-1, ZiYuan-1, ZiYuan-3 (Kirk et al., 2008; Sun et al.,2015; Jiang et al.,2014; Tong et al., 2015a, 2015b, 2015c, 2015d, 2017, 2019; Wang et al.,2016; Pan et al., 2017; Zhu et al., 2018).

The choice of matching method directly affects the result of jitter detection. The phase correlation method can estimate the precise offset value between images, and it can be extended to high-precision dense matching between images by sliding window. At present, many scholars have made researches on the matching algorithm. The peak evaluation formula (PEF) method enables estimation of image displacements with 0.1-0.01pixels accuracy based on one-dimensional sinc function fitting (Nagashima et al.,2006). An improved phase correlation, which is based on 2-D plane fitting and the maximum kernel density estimator, combines the idea of Stone's method and robust estimator and increases the robustness when fitting the phase angle plane. (Tong et al., 2015c). And the SVD-RANSC subpixel phase correlation method integrates the advantages of Hoge's method and the RANSAC algorithm, avoiding the corresponding shortfalls of the original phase correlation method based only on SVD (Tong et al.,2015d).

It is generally believed that the matching window size affecting the jitter frequency detection. The maximum detectable frequency of ZiYuan-3 multispectral imagery can be up to

* Corresponding author

39.06 Hz ($\frac{sr}{2w}$, where the multispectral scanning rate sr is approximately 1250 Hz, the size of correlation window w is considered since the window is equivalent to low-pass filtering and is set as 16)(Ye et al., 2019). However, quantitative experimental analysis of matching window size on jitter detection has rarely been investigated.

Therefore, the purpose of this paper is to analyse the effect of image matching window size on jitter frequency detection based on simulation images, which are generated with a given short time lag and line scanning frequency affected by a modelled jitter. And the remaining parts of this paper are organized as follows. Following the introduction, the simulation images generation method and jitter detection method are presented in Section 2. And experiments and analysis of are described in Section 3. Finally, the conclusions are given in Section 4.

2. METHODOLOGY

2.1 Generation of jitter affected images

For generating of simulation images, we have to establish the digital simulation model which refers to the mathematical relationship between the ideal sampled image F and the final distortion image I (Zhuang.,2011).

$$F = \sum_{L=1}^{L_N}\sum_{R=1}^{R_N}\delta(x-La, y-Ra)f(x,y) \tag{1}$$

The degraded image caused by image shift and sampling is as follows:

$$T = \sum_{L=1}^{L_N}\sum_{R=1}^{R_N}\delta(x-La, y-Ra)f(x,y) * PSF(x,y) \tag{2}$$

Where PSF is the point spread function caused by image shift,

$$PSF(x,y) = \frac{1}{T}\int_{(R-1)T}^{RT}\delta(x-v(t-kT)-X(t), y-Y(t))dt \tag{3}$$

The ideal sample image of under the effect of image shift and sampling is as equation (4) and equation (5) (Zhuang, 2011, Tong., 2014):

$$I(R,C) = \frac{1}{T}\int_{(R-1)T}^{RT}F(Ra+v(t-(L-2+n)T, Ca+Y_{jitter}(t)dt \tag{4}$$

$$Y_{jitter} = \mathrm{A}\sin(2\pi ft+\varphi) \tag{5}$$

Where R = Row coordinates
C = Column coordinates
T =line integral time
F = ideal sample image
I =Simulated distorted image
Y_{jitter} = the distortion of jitter
a = the sampling interval, which is a pixel size
A =the amplitude of jitter
f = the frequency of jitter
φ =the phase of jitter

2.2 Image based jitter detection

According to the principle of jitter estimation based on parallax images, relative image distortions of multi-temporal images with some imaging time interval can be denoted as formula (6) (Teshima, Iwasaki, 2008)

$$\varphi(t) = j(t+\Delta t)\text{-}j(t) \tag{6}$$

Where t = imaging time
Δt = imaging time interval
$j(t)$ =the geometric displacement values
$\varphi(t)$ =the parallax values

Generally, the image distortions resulted from attitude jitter can be modelled as a sum of the sinusoidal functions with different amplitudes, phases, and frequencies. To simplify the derivation, it is assumed that the jitter contains only a single frequency, which can be denoted as follows:

$$j(t) = \sum_{i=1}^{N}A_j\sin(2\pi f_j t+\phi_j) \tag{7}$$

Where A_j , f_j , and ϕ_j denote the amplitude, frequency, and phase of the ith component of absolute jitter distortions, respectively. The relative residuals can also be expressed in a similar form as follows:

$$\varphi(t) = \sum_{i=1}^{N}A_\varphi\sin(2\pi f_\varphi t+\phi_\varphi) \tag{8}$$

Where A_φ , f_φ , and ϕ_φ denote the amplitude, frequency, and phase of the ith component of parallax difference value, respectively.

According to the synthesis and decomposition characteristics of the same frequency vibration (Liu et al., 2019), we can get the equation (9).

$$\begin{aligned} f_j &= f_\varphi \\ A_j &= A_\varphi / \sqrt{2-2\cos(2\pi f_j\Delta t)} \\ &= A_\varphi * \left|\frac{1}{2\sin(\pi f_j\Delta t)}\right| \end{aligned} \tag{9}$$

Therefore, the quantitative relationship between the jitter displacement and jitter parallax is determined.

It is worth noting that the frequency component of jitter should meet the equation (10), and it is difficult to detect the jitter information at the integral times of the blind spot frequency from the parallax image.

$$f_j \neq \frac{n}{\Delta t}(n=1,2,3\cdots) \tag{10}$$

Moreover, when the jitter frequency is close to the integral multiple of the characteristic frequency. We can get the follow equations (11)and (12):

$$f_j = \frac{n+\Delta n}{\Delta t}, \Delta n \to 0 \tag{11}$$

$$A_j = A_\varphi * \frac{1}{2\sin(\pi \Delta n)} \tag{12}$$

In the case of the same image quality and content richness, the imaging position difference at different frequencies is obtained by the image registration method. It can be approximately considered that the amplitude error of imaging position difference at different frequencies is the same, which is expressed by α . According to the error synthesis equations, the vibration amplitude error caused can be expressed as equation (13):

$$\alpha_j = \alpha_\varphi * \frac{1}{2\sin(\pi \Delta n)}, \Delta n \to 0 \tag{13}$$

Therefore, when the frequency is close to the blind spot frequency, the error of transfer coefficient between the jitter and the parallax is much greater than 1, which greatly enlarges the error of the imaging position difference, leading to the increase of jitter error.

2.3 The phase correlation algorithm based on PEF

The basic principle of phase correlation algorithm based on PEF (peak evaluation formula) is to use two-dimensional sin function fitting the peak matrix of cross power spectrum after inverse transformation, and getting accurate sub-pixel matching results according to the fitting results (Nagashima et al.,2006).

If the reference image $m(i, j)$ and the matched image $s(i, j)$ have a displacement (x_0, y_0) in the row and column direction in the airspace, the expression of the cross-power spectrum obtained by the correlation between the reference image and the image to be matched is:

$$Q(u,v) = \frac{M(u,v)S^*(u,v)}{\left|M(u,v)S^*(u,v)\right|} = \exp\{-i(ux_0 + vy_0)\} \tag{14}$$

The result of inverse Fourier transform is a peak matrix. The coordinate position corresponding to the peak value is the whole pixel matching position of the matched image relative to the reference image. And the equation of the peak matrix can be approximately expressed as follows:

$$q(i, j) \cong \frac{\sin\{\pi(i + x_0)\}}{\pi(j + x_0)} \frac{\sin\{\pi(j + y_0)\}}{\pi(j + y_0)} \tag{15}$$

Its peak value matrix $q(i, j)$ can be approximately expressed by the above formula under ideal conditions. Therefore, by performing two-dimensional fitting on the peak matrix in two directions respectively, we can get accurate fitting peak vertices, and then get sub-pixel matching results.

2.4 The experimental workflow

High precision dense matching is the foundation of jitter detection. Therefore, we obtained lots of high-precision image points by point dense matching strategy of the PEF phase correlation. And the Figure 1 shows the workflow of the proposed method.

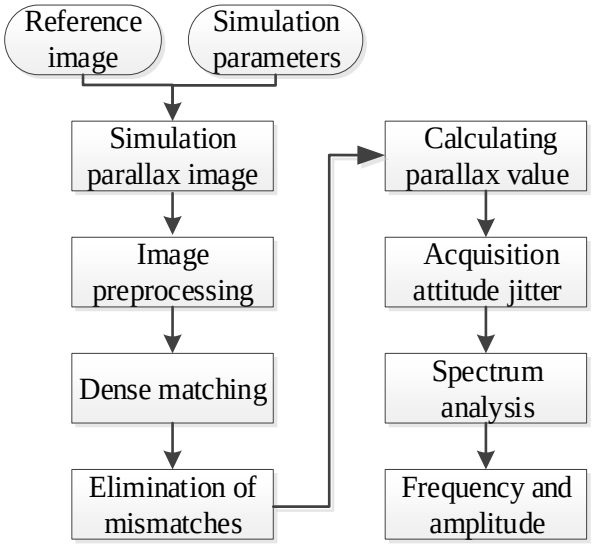

Figure 1. Overall workflow of the proposed method

The main processes are as follows:

(1) Simulation image generation: Based on the method shown in 2.1, two images with different imaging time are generated by adding jitter in the cross direction.

(2) Image pre-processing: Based on the generation method of 2.1, we generated two parallax images of different time. And to ensure the reliability of dense matching, we used Wallis filter for enhancing the image and improving image contrast (Barazzetti, Scaioni, 2010). The known disparity structure is used for initial image registration to eliminate the fixed offset between two images.

(3) Image dense matching: The correlation window size is set to oblong shape in order to estimate the relative registration error in the cross-track direction with a high time resolution, which makes analysis robust to scene features (Teshima, Iwasaki, 2008), and the sub-pixel offset is calculated by normalized cross correlation (NCC) (Barnea and Silverman, 1972) for coarse matching and PEF phase correlation method for accurate matching, so parallax images in two directions can be generated.

(4) Eliminating mismatch results: Before the follow-up analysis, it is necessary to eliminate mismatches and reduce the impact of noise. Firstly, setting threshold value to remove the abnormally large offset value in the disparity image. Secondly, the normalized correlation coefficient between matching windows is calculated to remove the low texture or low correlation area whose correlation coefficient is less than the threshold value of 0.7. The fitting residual value, returning by RANSAC robust estimation algorithm in the sub-pixel phase correlation calculation process, is used to eliminate the data of correlation quality difference. The image points on the same line are affected by the same jitter, so the outliers of each line are eliminated according to the principle of three times of mean square error.

(5) Obtaining jitter information: According to section 2.2, rebuilding of the jitter components, and converting to jitter information.

3. EXPERIMENTS AND ANALYSIS

To study the effect of image matching window size on satellite jitter frequency detection, simulation experiments are carried out. The reference image is from a panchromatic image of ZiYuan-3 satellite in Figure 2, which size is 1280*1280 pixels, and the simulation parameters are shown as Table 1.

Figure 2. Reference image

Simulation Parameter	Value
Line scanning time(s)	0.00020
time lag (lines)	135
Added jitter frequency (Hz)	50-2500

Table 1. Simulation parameters

3.1 Generation of jitter affected images

For verifying the method of jitter detection, two simulation images with a given short time lag and line scanning frequency affected by a modelled jitter are generated based on the principle of dynamic imaging process, where the line scanning time is 0.0002s, the time lag is 135 lines. And based on line scanning time and Nyquist's law, the detectable frequency is no more than 2500 Hz, so we add jitter in the column direction with frequency varying from 50 Hz to 2500 Hz.

According to the principal of dynamic imaging in section 2.1, (1) we first load the reference image; (2) The simulation parameters are substituted into the dynamic imaging model;(3) we can calculated the coordinates of image points at each time and the position of the point may no longer be an integer, so we do bicubic convolution interpolation (Keys, 1981); (4) Traversing the whole image, we can obtain two multi-temporal images affected by a modelled jitter as shown in the Figure 3.

(a) Simulation image 1 (b) Simulation image 2

Figure 3. Multi-temporal images which affected by a modelled jitter.

3.2 Analysis of effect of matching window size on jitter detection

To analyse the effect of the matching window size for jitter detection, we change the size of the matching window in the along-track direction, which is 128 pixels (cross)*16 pixels (along), 128 pixels (cross)*32 pixels (along), 128 pixels (cross)*64 pixels (along).

After carrying out multi-temporal image dense matching and removing mismatch, we obtained the relative disparity curves which are averaged the disparity maps at each line. The results of dense matching with three different match size are presented in Table 2, as shown in Table 2, jitter frequency as high as 2475 Hz can be effectively detected with all the three matching window size, but it failed for the detection of 2500 Hz, with the detected frequency as 2475Hz. The reasons may be that, the sampling frequency is closer to Nyquist sampling frequency, the aliasing effect will appear, that is, the frequency component higher than half of the sampling frequency is reconstructed into the signal lower than half of the sampling frequency.

Frequency (Hz)	Detected Frequency (Hz)		
	Matching window size (cross*along)		
	128*16	128*32	128*64
50	50	50	50
250	250	250	250
650	650	650	650
1050	1050	1050	1050
1250	1250	1250	1250
1450	1450	1450	1450
1850	1850	1850	1850
2250	2250	2250	2250
2450	2450	2450	2450
2475	2475	2475	2475
2500	2475	2475	2475

Table 2. Jitter frequency detection results with different matching window size

For further discussion, 50Hz, 1250Hz parallax and spectrum analysis results are shown in Figure 4-Figure 9. In the Figure 4-6, we simulated the frequency of jitter is 50Hz, and it is clearly we can detect 50Hz successfully with different matching size. And combined with Figure4-9 and Table 2, we can draw the conclusion that the detectable frequency is almost not affected by the image matching window size.

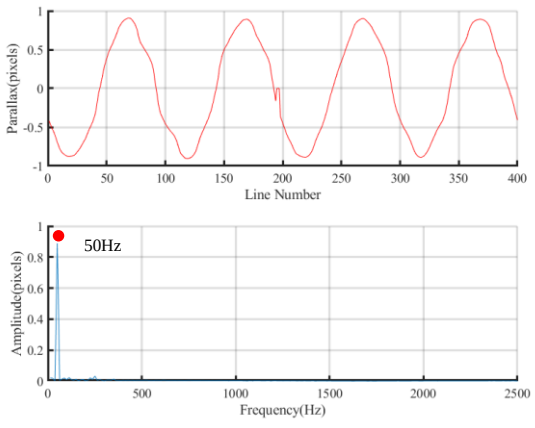

Figure 4. Parallax curve with simulated jitter frequency of 50 Hz, matching window size is 128(cross)* 16 (along)

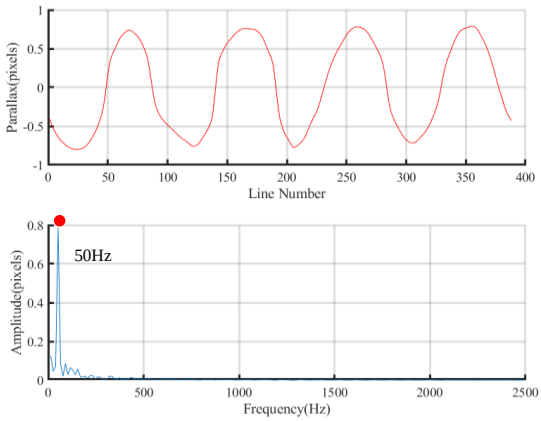

Figure 5. Parallax curve with simulated jitter frequency of 50 Hz, matching window size is 128(cross)* 32(along)

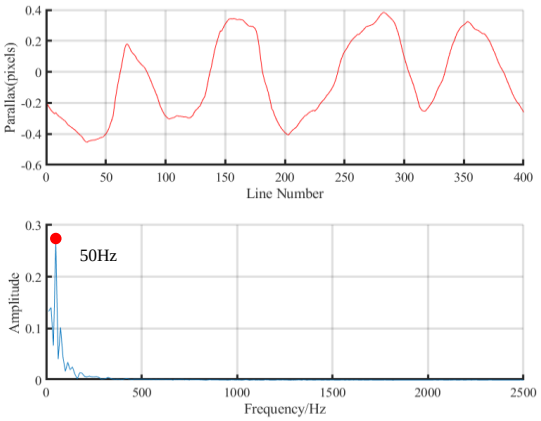

Figure 6. Parallax curve with simulated jitter frequency of 50 Hz, matching window size is 128(cross)* 64(along)

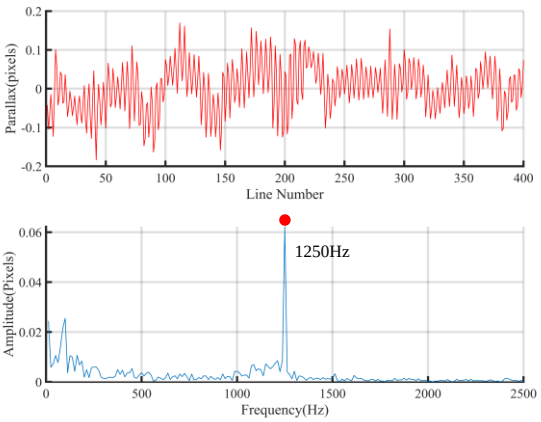

Figure 7. Parallax curve with simulated jitter frequency of 1250 Hz, matching window size is 128(cross)* 16 (along)

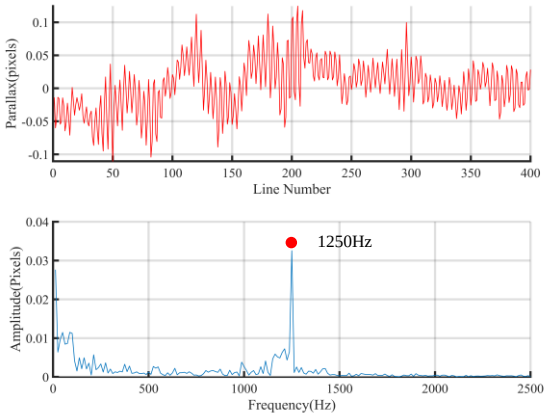

Figure 8. Parallax curve with simulated jitter frequency of 1250 Hz, matching window size is 128(cross)* 32(along)

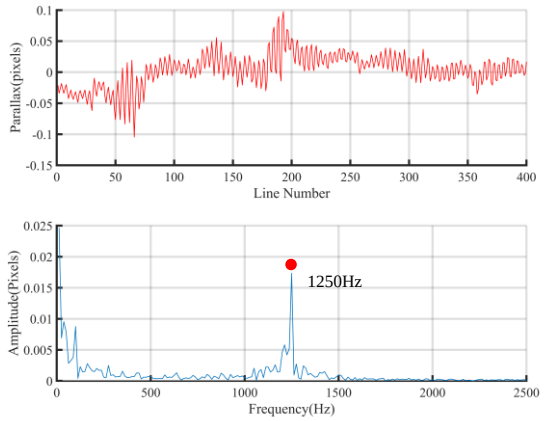

Figure 9. Parallax curve with simulated jitter frequency of 1250 Hz, matching window size is 128 (cross)*64(along)

4. CONCLUSIONS

The satellite jitter is one of the key problems affecting the ability of high-precision observation and mapping. This paper studied the effect of matching window size on jitter frequency detection. The experimental study demonstrated the feasibility and reliability of high frequency jitter detection based on multi-temporal image matching. And, it indicated that the maximum detectable jitter frequency is almost not affected by the image matching window size. For simulated images with scanning rate of 5000 lines per second, the maximum detectable jitter frequency can be as high as 2475 Hz, close to the theoretical maximum detectable frequency of 2500 Hz, which provides useful demonstration for image-based satellite jitter detection capacity.

ACKNOWLEDGEMENTS

This work was supported by the National Key Research and Development Program of China (Grant No. 2017YFB0502903), the National Natural Science Foundation of China (Grant Nos. 41771483 and 41401531), and the Fundamental Research Funds for the Central Universities.

REFERENCES

Barazzetti, L., Scaioni, M., 2010. Development and Implementation of Image-based Algorithms for Measurement of Deformations in Material Testing. *Sensors* 10, 7469–7495.

Barnea, D.I., Silverman, H.F., 1972. A Class of Algorithms for Fast Digital Image Registration. *IEEE Transactions on Computers* C–21, 179–186.

Grodecki, J., Dial, G., 2003. Block Adjustment of High-Resolution Satellite Images Described by Rational Polynomials. *Photogrammetric Engineering & Remote Sensing* 69, 59–68.

Jiang, Y., Zhang, G., Tang, X., Li, D., Huang, W., 2014. Detection and Correction of Relative Attitude Errors for ZY1-02C. IEEE Transactions on Geoscience and Remote Sensing 52, 7674–7683.

Kirk, R.L., Howington-Kraus, E., Rosiek, M.R., Anderson, J.A., Archinal, B.A., Becker, K.J., Cook, D.A., Galuszka, D.M., Geissler, P.E., Hare, T.M., Holmberg, I.M., Keszthelyi, L.P., Redding, B.L., Delamere, W.A., Gallagher, D., Chapel, J.D., Eliason, E.M., King, R., McEwen, A.S., 2008. Ultrahigh resolution topographic mapping of Mars with MRO HiRISE stereo images: Meter-scale slopes of candidate Phoenix landing sites. Journal of Geophysical Research 113, pp. E00A24

Keys, R., 1981. Cubic convolution interpolation for digital image processing. *IEEE Trans. Acoust., Speech, Signal Process*. 29 (6), 1153-1160.

Liu, S., Tong, X., Wang, F., Sun, W., Guo, C., Ye, Z., Jin, Y., Xie, H., Chen, P., 2016. Attitude Jitter Detection Based on Remotely Sensed Images and Dense Ground Controls: A Case Study for Chinese ZY-3 Satellite. *IEEE Journal of Selected Topics in Applied Earth Observations and Remote Sensing* 9, 5760–5766.

Mattson, S., Boyd, A., Kirk, R.L., Cook, D.A., Howington-Kraus, E., 2009. HiJACK: Correcting spacecraft jitter in HiRISE images of Mars. Proceedings of the European Planetary Science Congress.

Nagashima S., Aoki T., Higuchi T., 2006. A subpixel image matching technique using phase-only correlation. Proceedings of the International Symposium on Intelligent Signal Processing and Communication Systems, Tottori, Japan, pp. 701-704

Pan, J., Che, C., Zhu, Y., Wang, M., 2017. Satellite Jitter Estimation and Validation Using Parallax Images. *Sensors* 17, 83.

Sun, T., Long, H., Liu, B.-C., Li, Y., 2015. Application of attitude jitter detection based on short-time asynchronous images and compensation methods for Chinese mapping satellite-1. *Optics Express* 23, 1395.

Takaku, J., Tadono, T., 2009. PRISM On-Orbit Geometric Calibration and DSM Performance. *IEEE Transactions on Geoscience and Remote Sensing* 47, 4060–4073.

Teshima, Y., Iwasaki, A., 2008. Correction of Attitude Fluctuation of Terra Spacecraft Using ASTER/SWIR Imagery with Parallax Observation. *IEEE Transactions on Geoscience and Remote Sensing* 46, 222–227.

Tong, X., Ye, Z., Xu, Y., Tang, X., Liu, S., Li, L., Xie, H., Wang, F., Li, T., Hong, Z., 2014. Framework of Jitter Detection and Compensation for High Resolution Satellites. *Remote Sensing* 6, 3944–3964.

Tong, X., Xu, Y., Ye, Z., Liu, S., Tang, X., Li, L., Xie, H., Xie, J., 2015a. Attitude Oscillation Detection of the ZY-3 Satellite by Using Multispectral Parallax Images. *IEEE Transactions on Geoscience and Remote Sensing* 53, 3522–3534.

Tong, X., Li, L., Liu, S., Xu, Y., Ye, Z., Jin, Y., Wang, F., Xie, H., 2015b. Detection and estimation of ZY-3 three-line array image distortions caused by attitude oscillation. *ISPRS Journal of Photogrammetry and Remote Sensing* 101, 291–309.

Tong, X., Xu, Y., Ye, Z., Liu, S, Li, L., Xie, H., Wang, F., Sa Gao, S., Stilla, U., 2015c. An Improved Phase Correlation Method Based on 2-D Plane Fitting and the Maximum Kernel Density Estimator. *IEEE Geoscience and Remote Sensing Letters* 12, 1953–1957.

Tong, X., Ye, Z., Xu, Y., Liu, S., Li, L., Huan X., Li T., 2015d. A Novel Subpixel Phase Correlation Method Using Singular Value Decomposition and Unified Random Sample Consensus. *IEEE Transactions on Geoscience and Remote Sensing* 53, 4143–4156.

Tong, X., Ye, Z., Li, L., Liu, S., Jin, Y., Chen, P., Xie, H., Zhang, S., 2017. Detection and Estimation of Along-Track Attitude Jitter From Ziyuan-3 Three-Line-Array Images Based on Back-Projection Residuals. *IEEE Transactions on Geoscience and Remote Sensing* 55, 4272–4284.

Wang, M., Zhu, Y., Pan, J., Yang, B., Zhu, Q., 2016a. Satellite jitter detection and compensation using multispectral imagery. *Remote Sensing Letters* 7, 513–522.

Wang, M., Zhu, Y., Jin, S., Pan, J., Zhu, Q., 2016b. Correction of ZY-3 image distortion caused by satellite jitter via virtual steady reimaging using attitude data. *ISPRS Journal of Photogrammetry and Remote Sensing* 119, 108–123.

Wang, M., Fan, C., Pan, J., Jin, S., Chang, X., 2017. Image jitter detection and compensation using a high-frequency angular displacement method for Yaogan-26 remote sensing satellite. *ISPRS Journal of Photogrammetry and Remote Sensing*130, 32–43.

Yang, B., Wang, M., Xu, W., Li, D., Gong, J., Pi, Y., 2017. Large-scale block adjustment without use of ground control points based on the compensation of geometric calibration for ZY-3 images. *ISPRS Journal of Photogrammetry and Remote Sensing*134, 1–14.

Ye, Z., Xu, Y., Tong, X., Zheng, S., Zhang, H., Xie, H., Stilla, U., 2019. Estimation and analysis of along-track attitude jitter of ZiYuan-3 satellite based on relative residuals of tri-band multispectral imagery. *ISPRS Journal of Photogrammetry and Remote Sensing*158, 188–200.

Zhuang, X., 2011. Analysis and Simulation of the influence of platform motion on the imaging quality of TDICCD camera Harbin University of Technology.

Zhang, G., Guan, Z., 2018. High-frequency attitude jitter correction for the Gaofen-9 satellite. *The Photogrammetric Record* 33, 264–282.

Zhu, Y., Wang, M., Cheng, Y., He, L., Xue, L., 2018. An Improved Jitter Detection Method Based on Parallax Observation of Multispectral Sensors for Gaofen-1 02/03/04 Satellites. *Remote Sensing* 11, 16.